FLUID MECHANICS SERIES

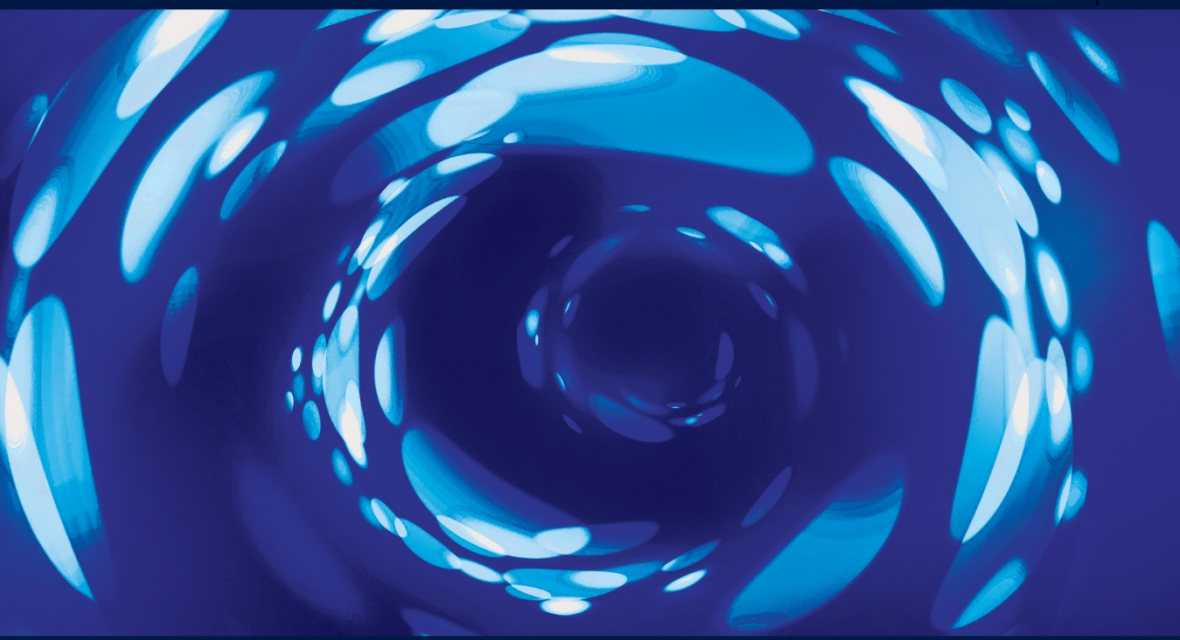

# Wall Turbulence Control

Sedat Tardu

iSTE WILEY

Wall Turbulence Control

# Wall Turbulence Control

Sedat Tardu

ISTE

WILEY

First published 2017 in Great Britain and the United States by ISTE Ltd and John Wiley & Sons, Inc.



ISTE Ltd
27-37 St George's Road
London SW19 4EU
UK

www.iste.co.uk

John Wiley & Sons, Inc.
111 River Street
Hoboken, NJ 07030
USA

www.wiley.com



Library of Congress Control Number: 2016959098

British Library Cataloguing-in-Publication Data
A CIP record for this book is available from the British Library
ISBN 978-1-84821-559-7

# Contents

# Preface

This short book is devoted to turbulent skin-friction control.

Reducing drag by only a few percent in transport vehicles (motor cars, aircraft, ships, etc.) would achieve a saving of tens of billions of Euros per year in fuel, and a significant reduction of the human impact on the environment. In the context of a civil or commercial transport aircraft, depending on the size, viscous or skin friction drag accounts for about 40–50% of the total drag under cruise conditions A cut in skin friction drag by 20% applied only to all commercial aircraft operating in the European Community would cut fuel consummation by about 30 million tones a year, corresponding to some 5–10% of total fuel consumption. This also corresponds to a reduction of several million tons of $CO_2$ emissions annually. It is also important to recall the main goals of the vision 2020 launched by the European commission: a 50% cut in $CO_2$ emissions per passenger kilometer. Environmental factors, such as noise, and impact on climate change, also have to be underlined. At present, the implementation of feasible, effective skin-friction control strategies is a long way from becoming a reality. It requires an in-depth knowledge of near-wall turbulence, which in spite of the considerable advances made during recent decades, is not yet at a sufficient level.

From a fundamental point of view, the management of the nonlinearity inherent in the Navier–Stokes equations coupled with the

complexity induced by the presence of the wall is a formidable challenge for the researchers.

The aim of this book is to give a short overview of the turbulent skin-friction research conducted up until now; however, in spite of the effort invested in its preparation, it is far from being exhaustive. Only a limited part of the very broad literature on the subject could be analyzed in this book. I must say that it is difficult to avoid a certain degree of subjectivity in the presentation of the existing control approaches, although I have tried to be as objective as possible.

The book contains four chapters. A general introduction is given in Chapter 1 wherein the key elements related to the tools necessary to develop control strategies, such as numerical simulations, micro sensors and actuators, are briefly discussed. The aim of Chapter 2 is to provide the reader with a short and concentrated review of the basic structural elements of wall turbulence. Passive control strategies are discussed in Chapter 3 that concentrate only on large eddy break-up devices, riblets and superhydrophobic surfaces. Active control of skin friction drag is the subject of Chapter 4, which aims to present the huge progress achieved in the domain over the last decades.

First and foremost, I would like to extend my thanks to my former PhD students, Olivier Doche, François Bouillon, Stéphane Montesimo and Frédéric Bauer, without whom I could certainly not undertake research in the fascinating area of flow control. Writing a book requires time. My heartfelt thanks go to my wife, Carmel, for her unfailing support, and to my sons, Aran, Noah and Teoman, for their patience.

Sedat TARDU
November 2016

# Notations

| | |
|---|---|
| $C_f$ | drag coefficient |
| $D/Dt$ | material derivative |
| $H$ | shape factor |
| $h$ | half-height of the channel |
| $k_x$ | streamwise wavenumber |
| $k_z$ | spanwise wavenumber |
| $\ell$ | mixing length |
| $\overline{P}$ | mean pressure |
| $p$ | fluctuating pressure |
| $\overline{u}_\tau$ | shear velocity ( $\sqrt{\overline{\tau}_w/\rho}$ ) |
| $U_i$ | local instantaneous velocity |
| $\overline{U},\overline{U}_1$ | mean streamwise velocity |
| $\overline{V},\overline{U}_2$ | mean wall-normal velocity |
| $\overline{W},\overline{U}_3$ | mean spanwise velocity |

| | |
|---|---|
| $\bar{U}_\infty$ | velocity outside of the boundary layer |
| $\bar{U}_c$ | velocity at the channel centerline |
| $\bar{U}_m$ | bulk velocity |
| $Re$ | Reynolds number |
| $Re_\tau$ | Reynolds number based on the shear-stress rate and the outer scale (von Kárman number) |
| $Re_\theta$ | Reynolds number based the momentum thickness and the velocity outside of the boundary layer (or velocity in the center of a channel) |
| $W_c$ | Coles' wake function |
| $u, u_1$ | streamwise fluctuating velocity |
| $v, u_2$ | wall-normal fluctuating velocity |
| $w, u_3$ | spanwise fluctuating velocity |
| $-\rho\overline{uv}$ | Reynolds shear stress (for the simplicity's sake, the correlation $-\overline{uv}$ is sometimes also called the Reynolds correlation) |
| $t$ | time |
| $x,\ x_1$ | streamwise coordinate |
| $y, x_2$ | wall-normal coordinate |
| $z\ , x_3$ | spanwise coordinate |
| $v_{Ko}$ | Kolmogorov velocity scale |

## Subscript and superscript notation

| | |
|---|---|
| $(\ )_i$ | velocity or vorticity component |
| $(\ )_w$ or $(\ )_0$ | quantity at the wall |

| | |
|---|---|
| $\overline{(\,)}$ | mean of a fluctuating physical quantity |
| $\overline{\overline{(\,)}}$ | Fourier transform |
| $(\,)^{+}$ | quantity rendered dimensionless by the inner scales $\overline{u}_{\tau}$ and $\nu$ |

## Vectorial operators

| | |
|---|---|
| $\vec{\nabla} = \frac{\partial}{\partial x_i}\vec{e}_i$ | $\vec{e}_i = \vec{i}, \vec{j}$ or $\vec{k}$, and the Einstein summation convention applies |
| $\nabla^2 = \frac{\partial^2}{\partial x_i \partial x_i}$ | divergence |
| $\bullet$ | scalar product |

## Greek symbols

| | |
|---|---|
| $\delta_{ij}$ | Kronecker delta |
| $\delta$ | boundary-layer thickness |
| $\delta_d$ | displacement thickness |
| $\delta_{\nu}$ | viscous sublayer thickness |
| $\delta_R$ | Rotta thickness |
| $\eta_{Ko}$ | Kolmogorov length scale |
| $\kappa$ | von Kárman constant |
| $\Lambda_0$ | outer length scale |
| $\nu$ | kinematic viscosity |
| $\nu_t$ | turbulent viscosity |
| $\mu$ | dynamic viscosity |
| $\nu$ | kinematic viscosity |

| | |
|---|---|
| $\bar{\Omega}_i$ | mean vorticity component *i* |
| $\bar{\Omega}_z$ | mean spanwise vorticity |
| $\omega_i$ | instantaneous local vorticity component *i* |
| $\omega_x, \omega_y, \omega_z$ | instantaneous local components of streamwise, wall-normal and spanwise vorticity |
| $\Pi$ | Coles' wake factor |
| $\rho$ | density |
| $\sigma_{ij}$ | stress tensor |
| $\sigma_{\tau_x'}$ | mean square value of fluctuations in wall shear stress in the streamwise direction |
| $\sigma_{\tau_z'}$ | mean square value of fluctuations in wall shear stress in the spanwise direction |
| $\sigma_{\omega_x}, \sigma_{\omega_y}, \sigma_{\omega_z}$ | mean square values of fluctuations in streamwise, wall-normal and spanwise vorticity |
| $\theta$ | momentum thickness |
| $\bar{\tau}_w, \bar{\tau}_0$ , $\bar{\tau}_x$ | mean wall shear stress |
| $\tau_w', \tau_0', \tau_x'$ | fluctuations of wall shear stress in the streamwise direction |
| $\tau_z'$ | fluctuations of wall shear stress in the spanwise direction |

# 1

# General Points

## 1.1. Introduction

The active control of wall shear stress (skin friction drag) in turbulent flows is a crucial industrial problem. For pipe and channel flows, 100% of the drag is due to skin friction. At subsonic cruising speeds, approximately half of the total drag of conventional aircraft and 90% of the total drag over an underwater vehicle are due to wall shear stress. A drag reduction of a few percent in civil aerodynamics, for instance, results in several billion dollars of fuel being saved, with a direct environmental impact. According to Kim [KIM 11], reducing fuel consumption by 30% through a drag-reducing control scheme would result in a saving of $38 billion a year for shipping industries. Fifty percent of aviation-related transport energy requirement is related to the turbulent skin-friction on commercial airliners [GAD 00] and the aviation consumes up to 13% of all energy used for transport. A cut in skin friction drag by 20% applied only to all commercial aircrafts operating in the European Community would prevert several million tons of $CO_2$ emissions annually. Successful passive and active turbulent skin-friction control strategies can thus lead to substantial financial and environmental benefits.

The tools necessary to understand near wall turbulence physics and to develop efficient control strategies are the main subjects of this

*Wall Turbulence Control,* First Edition. Sedat Tardu.

introductory chapter. We first discuss some issues arising from numerical simulations of fully developed turbulent wall flows. This is followed by a short discussion dealing with the progress made during recent decades in the realization of microsensors and microactuators.

## 1.2. Tools to analyze and develop control strategies

### 1.2.1. *Numerical simulations*

The analysis and development of active or passive control strategies requires the detailed resolution of the near wall turbulent flow field. Well-resolved direct numerical simulations (DNSs) constitute an essential tool for these aspects. The publication of the first DNS of a fully developed turbulent channel flow goes back to 1987 [KIM 87]. These data were generated in a small computational domain, and at a low Reynolds number of $Re_\tau = h^+ = \frac{h\overline{u}_\tau}{\nu} = 180$. Here, $h$ is the channel half width, $\overline{u}_\tau$ is the shear velocity and $\nu$ is the kinematic viscosity. The quantities scaled by the inner variables $(\overline{u}_\tau, \nu)$ are denoted as $(\ )^+$ hereafter. To our best knowledge, the last DNSs realized in a large domain, of sizes $L_x = 8\pi h$ in the streamwise and $L_z = 3\pi h$ in the spanwise directions, have recently been reported by Lee and Moser [LEE 15] and reached $Re_\tau = 5200$ corresponding to $Re = \frac{\overline{U}_m h}{\nu} = 1.25 \times 10^5$, where $\overline{U}_m$ is the bulk velocity. The computations were realized on an IBM BlueGene/Q system and have an excellent scalability up to 786,432 cores. The entire simulation was conducted over 9 months. Thus, the Reynolds number resolved by DNS increased by a factor of 30 in three decades, due to the progress in scientific computing technology.

However, the DNS of Lee and Moser [LEE 15] generated 140 Terabytes of data [LEE 14]. The management and analysis of this amount of data is delicate, and even the postprocessing requires massively parallelized codes and the use of supercomputers. This explains why the vast majority of the studies dealing with active and

passive control and using DNS is limited to low Reynolds numbers of about $Re_\tau = 200$, as we will see in the following chapters. Trying to cope with this problem by recourse to large eddy simulations (LESs) is obviously hopeless. The main reason is that, not only is the optimal control scheme only acceptable at the subgrid-scale in this case, but in addition the strategies developed by this approach are viable only if the near wall coherent structures are adequately resolved, which is not the case even if recently developed dynamic subgrid models are used. The same $Re$ number limitation is also inherent in experimental control investigations, mainly because of the necessity for performing measurements very close to the wall.

The Reynolds number dependence of the control strategies is undoubtedly an important issue. The effect of the large-scale outer structures on the wall shear stress turbulent intensity is relatively well understood by now (see [TAR 14] and the references within), but the role they play in the regeneration of the mean wall shear stress (drag) is unclear at the moment. Regarding the use of the direct numerical simulations, the DNS around $Re_\tau \equiv 1000$ obtained in large computational domains seems to be a good compromise. We will, however, see later on that the majority of existing active-passive control investigations are realized in much lower Reynolds number nowadays.

### 1.2.2. *Sensors*

The technical implementation of any drag active control method necessitates the use of microsensors and microactuators. Micro system technology has developed tremendously over the last decades. We will shortly review some aspects of microsensors and actuators in this section, which is mainly based on [TAR 10a]. The reader is referred to [GAD 05] for further details.

#### 1.2.2.1. *Pressure sensors*

Some quantities in near-wall turbulence appear, at first glance, to be simple to determine, quantify and analyze, but are actually phenomenally complex once we get into the details. Although one of

these quantities is the wall shear stress, the second is undoubtedly the pressure field. The fluctuating pressure field is directly linked to the hydro/aero-acoustic noise, as clearly shown in the classic analogy of Lightill [LIG 52, LIG 54]. The instantaneous pressure gradient has a direct influence on the structure of the wall flow in a turbulent boundary layer. The information contained in the pressure is global, as it is a volume integral containing instantaneous velocity gradients and a surface integral of the shear. Pressure/velocity correlations, in rapid and slow terms, play a vital role in transport equations [MAN 88, TAR 12].

The local instantaneous pressure gradients are related to the fluxes of vorticity at the wall through

$$\frac{\partial p^+}{\partial x^+}_0 = -\frac{\partial \omega_z^+}{\partial y^+}_0 \qquad \frac{\partial p^+}{\partial z^+}_0 = -\frac{\partial \omega_x^+}{\partial y^+}_0 \qquad [1.1]$$

where the subindex 0 refers to the wall as usual and $\omega_x$ and $\omega_z$ are the local instantaneous streamwise and spanwise vorticity components. The wall normal vorticity flux at the wall is zero, but its flux can be manipulated through

$$\frac{\partial \omega_y^+}{\partial y^+} = -\frac{\partial \omega_x^+}{\partial x^+} - \frac{\partial \omega_z^+}{\partial z^+}$$

An adverse local pressure gradient at the wall $\frac{\partial p_x^+}{\partial x^+} \geq 0$ plays the role of a sink of vorticity. Micropressure sensors adequately distributed at the wall can thus clearly be incorporated in any control active scheme to manipulate the vorticity fluxes at the wall.

It is, however, difficult to use the pressure information itself in an active control scheme unless we consider actuators and sensors distributed in the flow, or at the wall, which would specifically act on global characteristics. In isotropic homogeneous turbulence, the intensity of pressure fluctuations is linked to kinetic energy by a

function that depends slightly on the turbulent Reynolds number. This is given by

$$\overline{p^2} = p' = f\left(Re_\lambda\right)\rho\bar{K} \qquad [1.2]$$

where $Re_\lambda$ is the Reynolds number based on the Taylor scale, $\bar{K}$ *is* the kinetic energy and $\rho$ is the density [HIN 75]. The constant $f\left(Re_\lambda\right)$ varies between 0.6 and 0.8. The estimation of temporal and spatial scales of pressure fluctuations is difficult in inhomogeneous and anisotropic flows. Nevertheless, upper limits can be determined in wall flows using the previous relation and the maximum kinetic energy in the internal layer. We therefore have

$$p'^{+} = \frac{p'}{\rho u_\tau^2} \approx C k_{\max}^{+} \approx 3$$

where we have assumed that $k_{\max}^{+} \approx 4$, at the distance $y^{+} = 12$ from the wall, and that $C = 0.75$. The constant $C$ increases with the Reynolds number, varies between 0.5 and 1, and we consider its median. If to simplify, we opt for a Gaussian distribution of the pressure fluctuations, the sensor has to be able to depict values up to $\pm 10 p'$, implying a sensitivity of the sensor of about $s_{p'}^{+} \approx \pm 30$.

In isotropic homogenous turbulence, the spatio-temporal pressure correlations implicitly contain the Taylor scale $\lambda$ related to the longitudinal velocity correlations [HIN 75, p. 309]. The $p$ length scale must be somewhat linked to $\lambda$, and the most critical value in the wall layer is the Taylor scale at the wall [ANT 91]. In fact, in the viscous sublayer, dissipation is approximately equal to $\varepsilon \approx \frac{5}{4}\nu\overline{\left(\frac{\partial u}{\partial y}\right)^2} \approx \frac{5}{4\rho}\overline{\tau'\tau'}$, where we used the asymptotic value of $\overline{\left(\frac{\partial u}{\partial y}\right)^2}$ at the wall. The corresponding Taylor scale in the wall

normal direction varies, as $\lambda_y^+ \approx \frac{5}{4} y^+$ when $y^+ \to 0$. The intensity of the wall pressure fluctuations in the small-scale wave number range is inversely proportional to the thickness of the viscous sublayer. The resolution of the inner layer in its totality clearly requires probes that have a dimension $d^+$ that should not exceed five wall units. This statement is in agreement with the conclusion of [GAD 94], involving general Reynolds number dependency of sensor sizes in wall turbulent flows. In order to better describe the effect of probe size on resolution, Figure 1.1 shows the distribution of the intensity of pressure fluctuations reported to the wall shear-stress $\sigma_p^+ = \sqrt{\overline{pp}} \big/ \rho \overline{u}_\tau^2$ versus the size of the probe $d^+$, in the range $4.10^3 \le \mathrm{Re}_\theta \le 5.10^3$. We notice a large, inevitable decrease in pressure fluctuations for sensors whose size exceeds the thickness of the viscous sublayer. This decrease is clearly due to the spatial averaging effect of active and passive eddies of the buffer layer.

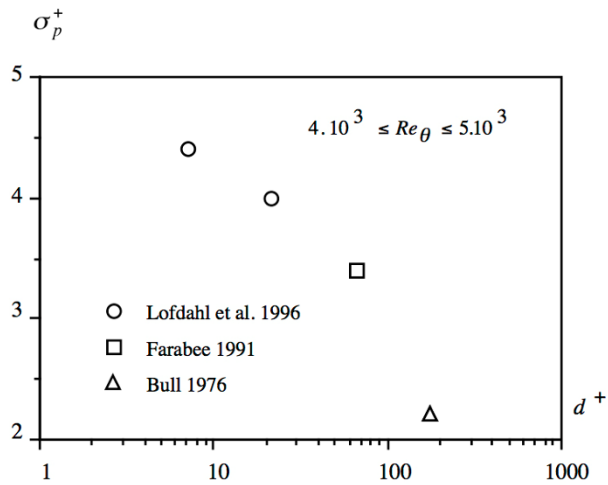


**Figure 1.1.** *The sensor size effect on the measured pressure intensity*

The frequency response of the sensor should be $f^+ = 1/\eta^+$ where $\eta$ is the Kolmogorov length scale, which is $\eta^+ \approx 1.5$ in the viscous

sublayer, leading to $f^+ \approx 0.7$. The spacing of the pressure sensors in the network configuration in the viscous sublayer should typically be $e^+ \leq 10$. The largest wavenumber that can be analyzed using a sensor of streamwise extend $d^+$ is $k_x^+ = 2/d^+$. Table 1.1 shows the size and spacing of the pressure sensors in physical units for a turbulent boundary layer at a small (mild) Reynolds number based on the boundary layer thickness of $\mathrm{Re}_\delta = 4.10^4$ (corresponding to the Reynolds number based on the momentum thickness of $\mathrm{Re}_\theta = 5000$). It can be clearly seen that the conditions are severe, particularly since $\mathrm{Re}_\delta = 4.10^4$ given in Table 1.1 is rather for academic purposes[1] and it is three order of magnitudes smaller than the Reynolds number based upon the fuselage length of an Airbus 320 in cruise conditions.

| | *Sensitivity* | *Dimensions* | *Frequency response* | *Spacing between sensors in a given network* |
|---|---|---|---|---|
| *WALL UNITS* | $s_{p'}^+ = \pm 30$ | $d^+ \leq$ 5 to 10 | $f^+ = 0.7$ | $e^+ \leq 10$ |
| *PHYSICAL DIMENSIONS* Boundary layer at $\mathrm{Re}_\theta = 5000$ | $s_{p'} = \pm 11$ Pa | $d \leq 125$ to 250 µm | $f = 16$ kHz | $e \leq 250$ µm |

**Table 1.1.** *Required characteristics of pressure sensors in wall bounded turbulent flows at a small-moderate Reynolds number*

The principle of capacitive pressure sensors is the same as the microphone (Figure 1.2). The first MEMS capacitive sensor emerged early in the 1990s [HOH 89]. The advantages of this type of sensor are, on one hand, their adequate sensitivity to pressure fluctuations, and on the other hand their insensibility to temperature. On the other hand these sensors have relatively large dimensions, in the order of six times the thickness of the viscous sublayer in a turbulent boundary

1 This is indeed the lower limit of the Reynolds number with $Re_\tau = \delta^+ \approx 2000$ for the emergence of a clear logarithmic region; see [TAR 11a, TAR 14].